

High-speed, high-sensitivity, gated surface profiling with closed-loop optical coherence topography

Andrei V. Zvyagin, Ilos Eix, and David D. Sampson

We describe and experimentally demonstrate a novel (to our knowledge) surface profiling technique, for which we propose the term closed-loop optical coherence topography. This technique is a scanning beam, servo-locked variation of low-coherence interferometry. It allows for the sub-wavelength-resolution tracking of a weakly scattering macroscopic-scale surface, with the surface profile being directly output by the controlling electronics. The absence of significant real-time computational overhead makes the technique well suited to high-speed tracking. The use of a micrometer-scale coherence gate efficiently suppresses signals arising from structures not associated with the surface. These features make the technique particularly well suited to real-time surface profiling of *in vivo*, macroscopic biological surfaces. © 2002 Optical Society of America

OCIS codes: 170.1650, 120.6650, 110.4500, 120.3180.

1. Introduction

The real-time profiling of macroscopic biological surfaces *in vivo* is an important example of a noncontact surface profiling technique for which a number of demanding requirements must be met. These requirements include: detection of weak diffuse scattering; full profile measurement on subsecond to millisecond time scales for the avoidance of motion artifacts; as well as micrometer-scale axial sectioning to discriminate against reflections from nearby structures. This combination of requirements presents a challenge for existing surface profiling techniques. In this paper, we propose and demonstrate an interferometric optical tracking technique that can potentially fulfill these requirements.

Conventional techniques, such as phase-shifting interferometry¹ and white-light interferometry^{2,3} require substantial post processing to determine surface profiles, considerably hindering the realization

of real-time profiling. Optical coherence tomography is another technique that has recently shown great promise for *in vivo* imaging of both weakly and strongly scattering biological objects.⁴ However, real-time surface profiling by use of optical coherence tomography is impeded because it is necessary to record an entire three-dimensional data cube from which the surface profile can be extracted.⁵

Optical tracking of the surface of interest is an alternative and potentially high-speed approach, because the measured signals directly specify the location of the surface without the acquisition of excess data or of further computation. This approach generally relies on maintaining an optical-path difference between the sample surface and an actuator element, which is held to a preset constant value by use of a closed-loop servo-control. The surface profile is acquired by monitoring both the control signal and the lateral position of the probe beam as it is scanned across the sample. An example of this optical-tracking technique can be found in the non-interferometric focus detection method.⁶ While this method has recently been applied to real-time surface profiling, its application is likely to be limited to that of measuring specular reflection from surfaces.

Optical-tracking techniques based on interference are of great importance for the profiling of weakly scattering surfaces. The attractiveness of these techniques stems from the high sensitivity afforded by heterodyne detection as well as the subwavelength

The authors are with The University of Western Australia, Optical + Biomedical Engineering Laboratory, Department of Electrical and Electronic Engineering, 35 Stirling Highway, Crawley, Western Australia 6009. A. V. Zvyagin's e-mail address is azvyagin@ee.uwa.edu.au.

Received 18 July 2001; revised manuscript received 2 January 2002.

0003-6935/02/112179-06\$15.00/0

© 2002 Optical Society of America

axial resolution afforded by the interference fringes. The interference signal at the output of a two-path interferometer is used to establish phase lock between the reference and sample arms resulting in the optical path in the reference arm varying in accordance with the optical path in the sample arm. Several applications of so-called phase-lock interference microscopy to real-time surface profiling have been reported.^{7,8} The tracking performance of this technique is prone to cross talk due to coherent interference generated by laser light backscattered from structures unrelated to the surface of interest. In order to eliminate cross talk, phase-locked confocal interference microscopy has been proposed and demonstrated.^{9,10} This method makes use of confocal axial sectioning (gating) for discriminating contributions from different structures. Its performance depends on dynamically synchronizing the locations of the confocal gate and the phase lock point while tracking the surface profile. If the confocal gate is simply held fixed, the attainable tracking range will be limited to the confocal-gate width (ordinarily, several micrometers). The ability to move this gate synchronously with the coherence gate at sufficient speed over millimeter-scale distances is, to our knowledge, yet to be realized.

In this paper, we propose a novel interferometric optical-tracking technique, which we term closed-loop optical coherence tomography (closed-loop OCT), which circumvents the limitations of the previous methods. As a beam is scanned across the surface of a sample terminating one arm of a Michelson interferometer, a constant optical path difference is maintained between the reference and sample arms using an actuator in a servo loop controlled by feedback from the detected intensity. Closed-loop OCT benefits from the high-sensitivity and subwavelength resolution of conventional phase-locked interferometry, and it is further enhanced by use of a broadband light source. This broadband source enables a narrow coherence gate, typically some 10–20 micrometers in width, to be centered on the surface of interest, resulting in the elimination of cross talk from detected backscatter originating from outside this gated zone. The coherence gate is significantly more effective in rejecting these unwanted signals than the confocal gate in confocal interference microscopy.¹¹ The rest of this paper is organized as follows: In Section 2 the principles of operation of closed-loop OCT are described, and in Section 3 an experimental realization is outlined. In Section 4 experimental results that demonstrate the basic feasibility of the technique are presented, and in Section 5 the merits and limitations of the technique are discussed before concluding in Section 6.

2. Basic Principles

Closed-loop OCT may be thought of as a hybrid of phase-locked interferometry and optical coherence tomography. It comprises a setup identical to optical coherence tomography with the addition of a servo system. A schematic diagram of the system is

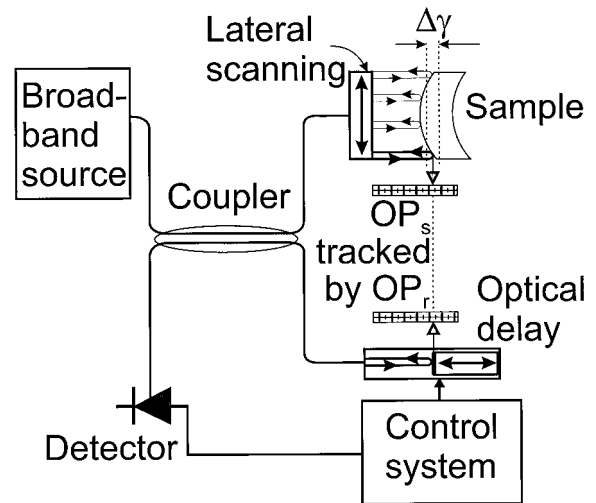


Fig. 1. Schematic diagram of a closed-loop OCT. OP_s , OP_r denote the optical path in the sample and reference arms, respectively; $\Delta\gamma$ denotes the coherence-gate width.

shown in Fig. 1. We first describe conventional optical coherence tomography and then describe the modifications required for closed-loop OCT.

The key subsystem is a Michelson interferometer in which light is split into two paths. An optical delay line that is used to vary the path length terminates one path, known as the reference arm. The other path, known as the sample arm, is terminated by the sample. A light source with a broad optical bandwidth is used so that at the output of the interferometer coherent interference takes place only when the two paths are closely matched. The detected photocurrent at the output of the interferometer, i_d , is a function of the modulus of the complex degree of coherence, $|\gamma(\Delta z)|$, where Δz denotes the optical-path difference between the reference and sample arms, such that

$$i_d \propto \frac{R + 1}{2} + |\gamma(\Delta z)| \sqrt{R} \cos[2k_0\Delta z], \quad (1)$$

where R is the reflectivity of the sample, and $k_0 = 2\pi/\lambda_0$, where λ_0 is the mean wavelength of the source. In expression (1) perfect reflectivity in the reference arm and unity refractive index of all optical media in the reference and sample arms are assumed for convenience. As can be seen from expression (1), interference fringes, i.e., periodic fluctuations in the detected optical signal, are observed only over a small range of axial distance determined by the full-width at half maximum of the complex degree of coherence, $\Delta\gamma$, (typically 10–20 micrometers), termed the coherence-gate width. The interference fringes signify that a reflection exists at a location in the sample, which is determined by the length of the reference path, and the reflectivity at that location is given by the envelope of the fringes.

In optical coherence tomography, a line scan or A scan comprises a linear scan of reflectivity versus axial depth. By simultaneously raster scanning the

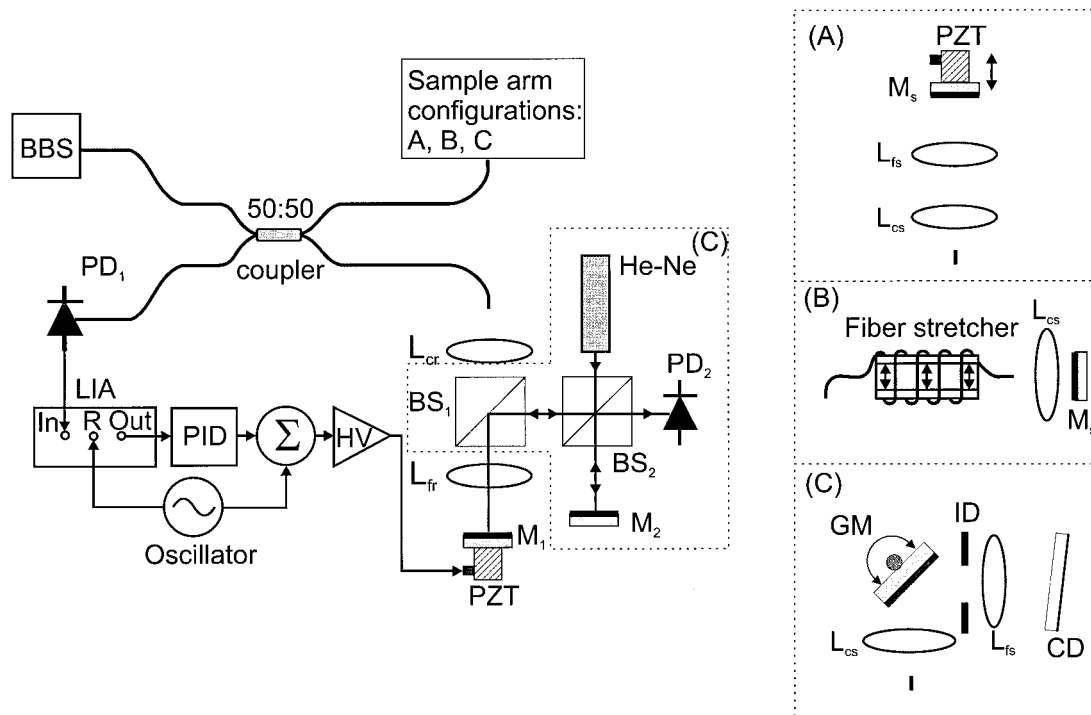


Fig. 2. Schematic diagram of experimental setup. BBS—broadband source; GM—galvanometer-mounted mirror; ID—iris diaphragm; BS—beamsplitter; PD—photodetector; M—plane mirror; He-Ne—helium-neon laser; LIA—lock-in amplifier; In, R, Out—input, reference, output terminals of the lock-in amplifier, respectively; PID—proportional-integral-differential controller.

beam transversely across the sample, a series of A scans are built up to form a two-dimensional B scan or tomograph of the reflectivity profile of a sample. A set of B scans recorded by scanning in the orthogonal lateral direction results in a three-dimensional morphological image. The topography of a surface of interest can be extracted from this data cube by suitable post processing. The axial resolution of the resulting profile is, in broad terms, determined by $\Delta\gamma$.

In closed-loop OCT, the beam is scanned laterally across the sample in two dimensions and a servo system simultaneously drives the optical-path length of the reference arm to match the location of the surface, which is thus continuously tracked. The topography of a surface of interest is obtained directly from the drive parameters of the scanning system and the control signal of the servo system. The axial resolution of the resulting profile is, in broad terms, determined by the fringe spacing $\lambda_0/2$.

The servo system in closed-loop OCT comprises an actuator and a servo controller. The first stage of the controller in our scheme employs a lock-in amplifier that synchronously detects an out-of-band amplitude modulation imparted to the detected photocurrent through the actuator. The lock-in amplifier conveniently eliminates sensitivity to the large direct current background represented by the first term in expression (1). The modulated optical-path difference, Δz_m , is then expressed by $\Delta z_m = \Delta z + \xi \cos f_m t$, where Δz is the initial offset, f_m is the reference frequency, and ξ is the reference amplitude, which must be kept small, i.e., $\xi \ll \lambda_0/2$. For max-

imum visibility, the initial offset Δz must be set to zero optical-path difference to the surface of interest, to well within the coherence-gate width, i.e., $\Delta z \ll \Delta\gamma$, and close enough to the zero crossing of a fringe to achieve initial lock. The lock-in amplifier outputs a signal, s , given by

$$s \propto \xi \sqrt{R} \left\{ \frac{d|\gamma|}{d(\Delta z_m)} \bigg|_{\Delta z_m = \Delta z} \cos[2k_0 \Delta z] - 2k_0 |\gamma(\Delta z)| \sin[2k_0 \Delta z] \right\}. \quad (2)$$

When $\Delta z \ll \Delta\gamma$, as required, the first term in the brackets is negligible and the error signal of the servo loop is given by

$$s \propto \xi \sqrt{R} |\gamma(\Delta z)| \sin[2k_0 \Delta z]. \quad (3)$$

The error signal is linearly proportional to Δz , provided that Δz remains locked to the zero crossing of a fringe, which facilitates simple and robust operation.

3. Experiment

The experimental setups are shown schematically in Fig. 2. The broadband light source comprises a fiber-coupled, high-power semiconductor optical amplifier that produces amplified spontaneous emission with a mean wavelength of 1.3 μm and a spectral width of 54 nm, giving a coherence-gate width of approximately 15 μm . The source illuminates a fiber-optic Michelson interferometer employing a cou-

pler that splits light equally into the sample and reference arms.

Three separate setups were used in the sample arm, as shown in Fig. 2. Setup (A) features a piezo-actuated mirror. Setup (B) features a piezoelectric fiber stretcher and mirror. Setup (C) features a galvanometer mirror used to laterally scan a weakly focused beam on a sample surface. In all three setups, the first lens, L_{cs} , serves to collimate light emerging from the fiber and, in setups (A) and (C), the second lens, L_{fs} (focal length 60 mm) serves to focus light onto the sample. The iris diaphragm, ID, is used to set the spot diameter on the sample, which was approximately 26 μm in our experiments. Setup (C) also incorporates a second interferometer in the reference arm for accurate calibration of the servo-actuator displacement. In this interferometer, light from a Helium-Neon laser is split into two paths. Mirror M_2 terminates the reference path and mirror M_1 terminates the sample path, which include reflections from beamsplitters, BS_1 and BS_2 , respectively. The beams from the sample and reference arms recombine on the detector, PD_2 , giving rise to the interference fringes used for calibration.

The reference arm uses the same combination of lenses used in the sample arm for setup (C). The use of these lenses in the reference arm compensates for the material dispersion induced by the lenses in the sample arm as well as ameliorates the effect of mirror wobble. Mirror wobble alters the coupling efficiency of light reflected back into the fiber from the mirror, M_1 , when the servo actuator is in motion. A 60- μm -range piezoelectric actuator-mounted mirror, PZT, was used as the servo actuator.

The electronic part of the servo control circuit consists of an oscillator, lock-in amplifier (LIA), proportional-integral-differential (PID)-controller, summer, and a high-voltage amplifier (HV), as shown in Fig. 2. The photocurrent from a PIN-diode receiver, PD_1 , is input to the lock-in amplifier operating at a reference frequency of $f_m = 14$ kHz. The output of the lock-in amplifier is input to the PID-controller, which generates the control signal. The control signal is summed with the reference signal and fed into the high-voltage amplifier, which drives the piezoelectric actuator. The bandwidth of the servo system is limited to approximately 1 kHz by the first mechanical resonance of the mirror-loaded actuator.

4. Results

To characterize the closed-loop OCT system, a plane mirror mounted on a piezoelectric translator was used to terminate the sample arm [set up (A) in Fig. 2]. The translator was driven with a 500-Hz triangular waveform, which corresponds to an axial slew rate of approximately 10 mm/s. Once phase lock was established, the system was observed to maintain closed-loop operation when tracking the quasi-linear periodic excursions of the mirror. An attenuator placed in front of the mirror in the sample arm was used to determine the acceptable return loss (i.e., the ratio of incident power to detected power), for

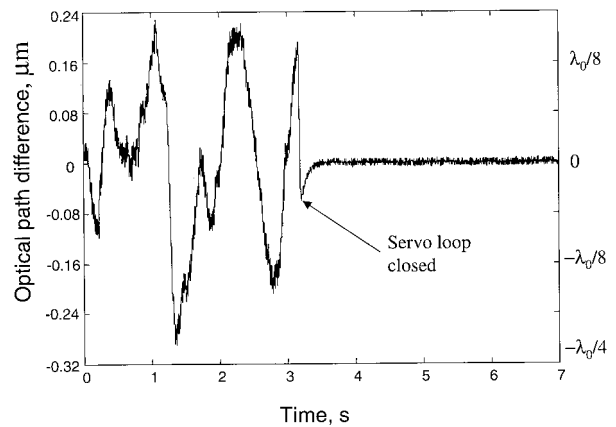


Fig. 3. Optical-path difference versus time before and after closing the servo control loop. Scale at right shows optical-path difference scaled by the mean wavelength of the source.

stable operation. The system could track the mirror with a return loss of as high as 60 dB, which is well below the return loss from typical biological surfaces (e.g., the return loss of the air-cornea interface is typically 40 dB¹²).

In a separate experiment using setup (B), a piezoelectric fiber stretcher was used to vary the optical-path difference in the sample arm. From this experiment, the dynamic axial resolution of the closed-loop OCT was determined to be better than 0.2 μm .¹³

Profiling of a diffusely scattering surface in close proximity to a second surface of similar reflectivity provides a more stringent test of the system. For this test employing setup (C) in Fig. 2, a compact disk was chosen as the sample, comprising an imprinted metallic layer overlaid by a 1.2-mm thick plastic protective layer. To avoid Fresnel reflections, the disk was tilted at approximately 3° with respect to the focal plane of the lens, L_{fs} . The disk was oriented so that the probe beam was incident on the plastic layer. To initiate surface profiling, the coherence gate was centered on the surface of interest, the imprinted surface. Consequently, the signal from the front surface was not detected. The beam was first directed to a fixed point on the disk. Figure 3 shows a typical trace displaying the time evolution of the output of the lock-in amplifier before and after closing the servo loop. Figure 3 shows the suppression of the free-running, mechanically induced fluctuations in the interferometer when operation in the closed-loop mode is initiated. Continuous closed-loop operation was maintained for periods of in excess of 1 h.

To generate a line profile with this system, the galvanometer mirror, GM, is used to scan the beam across the tilted surface of the compact disk causing optical-path variations that are compensated by the actuator mirror, M_1 . The line profile is obtained by recording the control signal at the output of the PID-controller versus the drive signal of the lateral scan. The resulting profile was found to suffer from inaccuracy due to the nonlinear and hysteretic response

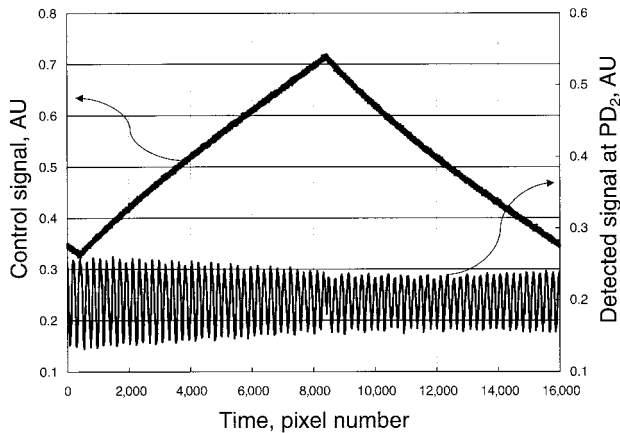


Fig. 4. Detected control signal (upper curve) and signal at photodetector PD₂ (lower curve) versus time as the probe beam scans across the tilted surface of the compact disk. AU—arbitrary units.

of the piezoelectric actuator. In order to correct for this inaccuracy, the reference interferometer shown in setup (C) was employed. The simultaneous recording of a line profile and the reference interference fringes, an example of which is shown in Fig. 4, enabled the recorded profile to be accurately calibrated by correction according to the measured fringe spacing. Figure 4 highlights the nonlinearity of the piezoelectric actuator.

Figure 5 shows two line-profile recordings: The first curve, labeled Closed-loop OCT, was obtained by correcting the surface profile recorded by the closed-loop system with the fringe spacings recorded by the reference interferometer. Data points, labeled OCT, represent the same line profile obtained using optical coherence tomography. For these measurements, a series of A scans across the surface was recorded along with the reference interference fringes. The maxima of the recorded interferograms were located with a peak search algorithm to determine the coordinates of the surface, which were subsequently corrected with the reference fringes. Comparison of the two curves shows excellent agreement. Indeed, the

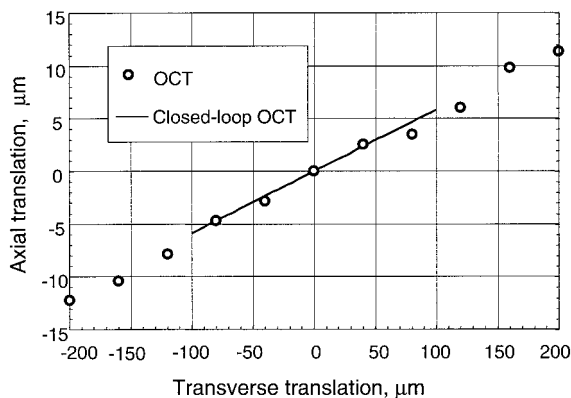


Fig. 5. Measured line profile of the surface of a tilted compact disk using closed-loop OCT (solid curve) and optical coherence tomography (open circles).

data demonstrate the superior axial resolution of closed-loop OCT over conventional optical coherence tomography. The speckle induced by the sample limited the range of the closed-loop system. This is discussed further in Section 5.

5. Discussion

Several issues remain to be investigated before closed-loop OCT can be considered as optimized for real-time surface profiling of biological media. The most important issue is speckle, which is manifested as random fluctuations in the magnitude of the interference signal. The detected signal arising from each discrete sampling volume (voxel) is made up of signals from each individual scatterer present within the voxel. Each individual scatterer's signal is characterized by its amplitude, a measure of its reflectivity, and its phase, a measure of its relative location within a voxel. The major effect of the random and uncontrollable amplitudes and phases of these individual signals is to impart an amplitude to the detected signal that varies randomly from voxel to voxel. The significance of this for closed-loop OCT is that these variations result in random variations of the slope of the transfer function of the servo loop, which can give rise to unstable operation.

In our experiments speckle-corrupted signals from several samples, which included glass slides and the compact disk, were observed to be broadly similar. The effect of speckle was ameliorated by the large spot diameter employed, which ensured that a large number of scatterers were included within a sample voxel. Detection of a large number of scatterers is known to limit the speckle's contrast.¹⁴ This enabled stabilization of the servo control to obtain the experimental results shown in Fig. 5 at the expense of lateral resolution—the compact disk's pit structure was not resolved.¹⁵ The profiling rate, however, did not exceed 25 ms per line, which is greater than an order of magnitude slower than that potentially achievable considering the intrinsic bandwidth of the servo control system. This result and the reduced range suggest that the effect of speckle on closed-loop operation warrants further study.

Another important aspect of closed-loop OCT is the speed requirement of the actuator. To quantify this requirement, the following example is considered. Assume a surface profile over a 1 mm × 1 mm area with a lateral resolution of 10 μm is acquired in 0.1 s, which ensures motion-artifact-free acquisition. The transverse scanning velocity of the probe beam required to achieve this is 2 m/s. A surface feature with a slope of 45° relative to the optical axis imposes an identical requirement on the slew rate of the servo system of 2 m/s. For surfaces with steeper features, higher slew rates are required. A medium-speed piezoelectric actuator, as used in our experiment, supports only a 50 mm/s slew rate. However, high-speed actuators based on electro-optic or acousto-optic effects can provide the required slew rates. For example, commercial acousto-optic deflectors can attain slew rates of up to 500 m/s.¹⁶

In several important applications, such as corneal profilometry, it is sufficient to sample the surface points sparsely to obtain the necessary information on its curvature. In addition, alternative surface-acquisition strategies to a raster scan (for example, employing radial or spiral scanning patterns) are also possible, including scanning patterns with lower-gradient trajectories chosen to suit the particular topography expected. The above factors can significantly reduce the requirements on the slew rate.

6. Conclusion

In summary, we have proposed a new closed-loop, servo-controlled mode of operation of optical coherence tomography that is suitable for high-speed, high-resolution surface profiling of macroscopic, millimeter-scale surfaces as encountered in real-time *in vivo* imaging of macroscopic biological surfaces. The basic feasibility of the proposed technique has been established by demonstrating real-time line profiling with sub-wavelength resolution of a test surface. The superior axial resolution of the scheme was demonstrated by benchmarking it against conventional optical coherence tomography. An important potential application of the proposed technique is to corneal profiling. A high-speed, sub-micrometer-resolution corneal topographer capable of profiling *in situ* could enable significant improvement in photorefractive-surgery treatments.¹⁷

References

1. K. Creath, in *Progress in Optics: Volume XXVI*, E. Wolf, ed. (North-Holland, Amsterdam, 1988), Chap. V.
2. L. Deck and P. de Groot, "High-speed noncontact profiler based on scanning white-light interferometry," *Appl. Opt.* **33**, 7334–7338 (1994).
3. J. P. Lesso, A. J. Duncan, W. Sibbett, and M. J. Padgett, "Surface profilometry based on polarization analysis," *Opt. Lett.* **23**, 1800–1802 (1998).
4. E. A. Swanson, J. A. Izatt, M. R. Hee, D. Huang, C. P. Lin, J. S. Schuman, C. A. Puliafito, and J. G. Fujimoto, "*In vivo* retinal imaging by optical coherence tomography," *Opt. Lett.* **18**, 1864–1866 (1993).
5. G. Häusler and M. W. Lindner, "'Coherence radar' and 'spectral radar'—new tools for dermatological diagnosis," *J. Biomed. Opt.* **3**, 21–31 (1998).
6. A. Bartoli, P. Poggi, F. Quercioli, and B. Tiribilli, "Fast one-dimensional profilometer with a compact disk pickup," *Appl. Opt.* **40**, 1044–1048 (2001).
7. D. C. Leiner and D. T. Moore, "Real-time phase microscopy using a phase-lock interferometer," *Rev. Sci. Instrum.* **49**, 1702–1705 (1978).
8. T. Suzuki, O. Sasaki, and T. Maruyama, "Phase-locked laser diode interferometry for surface profile measurement," *Appl. Opt.* **28**, 4407–4410 (1989).
9. D. K. Hamilton and H. J. Matthews, "The confocal interference microscope as a surface profilometer," *Optik (Stuttgart)* **71**, 31–34 (1985).
10. H. J. Matthews, D. K. Hamilton, and C. J. R. Sheppard, "Surface profiling by phase-locked interferometry," *Appl. Opt.* **25**, 2372–2374 (1986).
11. J. A. Izatt, M. D. Kulkarni, H.-W. Wang, K. Kobayashi, and M. V. Sivak, "Optical coherence tomography and microscopy of gastrointestinal tissues," *IEEE J. Sel. Top. Quantum Electron.* **2**, 1017–1028 (1996).
12. E. A. Swanson, D. Huang, M. R. Hee, J. G. Fujimoto, C. P. Lin, and C. A. Puliafito, "High-speed optical coherence domain reflectometry," *Opt. Lett.* **17**, 151–153 (1992).
13. D. Silva, A. V. Zvyagin, and D. D. Sampson, "Closed loop optical coherence tomography for high speed profiling of macroscopic biological surfaces," in *Proceedings of the 12th Conference of the Australian Optical Society*, (Australian Optical Society, ISBN 0-7340-1737-5), p. 8, Sydney, (1999).
14. J. D. McKinney, M. A. Webster, K. J. Webb, and A. M. Weiner, "Characterization and imaging in optically scattering media by use of laser speckle and a variable-coherence source," *Opt. Lett.* **25**, 4–6 (2000).
15. S. R. Chinn and E. A. Swanson, "Multi-layer optical readout using direct of interferometric detection and broad-bandwidth light sources," *Opt. Memory Neural Networks* **5**, 197–217 (1996).
16. See, for example, A. A. Sa., Model AA.DTS.X-400, at <http://www.a-a.fr>.
17. S. Markos, "Refractive Surgery and Optical Aberrations," *Opt. Photon. News* **12**, 22–25, (2001).